

Article

# Charge Exchange Cross Sections for Noble Gas Ions and N<sub>2</sub> between 0.2 and 5.0 keV

Steven Bromley <sup>\*</sup>, Corey Ahl, Chad Sosolik and Joan Marler 

Department of Physics and Astronomy, Clemson University, Clemson, SC 29634, USA; cdahl@g.clemson.edu (C.A.); sosolik@clemson.edu (C.S.); jmarler@clemson.edu (J.M.)

\* Correspondence: sjbroml@clemson.edu

Received: 30 June 2019; Accepted: 8 October 2019; Published: 14 October 2019



**Abstract:** Charge transfer of an electron from a neutral atom to an ion is a fundamental interaction that plays a dominant role in the energy balance of atmospheric and astrophysical plasmas. The present investigation measured the charge exchange cross sections of noble gas ions (He<sup>+</sup>, Ne<sup>+</sup>, Ar<sup>+</sup>, Kr<sup>+</sup>) with N<sub>2</sub> in the intermediate energy range 0.2–5.0 keV. The systems were chosen because there remains a lack of consensus amongst previous measurements and regions where there were no previous measurements. A description of the mechanical design for an electrically floated gas cell is described herein.

**Keywords:** cross section; charge exchange; noble gas ions; N<sub>2</sub>; molecules; scattering

## 1. Introduction

Charge exchange between ions and neutrals is an important process in a number of fields including fusion science [1], astrophysics [2–5], and atmospheric physics [6–8]. Recently, charge exchange between stellar wind ions (H<sup>+</sup>, He<sup>+</sup>, He<sup>2+</sup>) and molecules has been investigated because of its relevance in astronomy e.g., with CO and CO<sub>2</sub> present in cometary atmospheres [9,10] and N<sub>2</sub> present in planetary atmospheres [11]. The charge exchange process is written



where ion A<sup>+</sup> carries the majority of the collision energy compared to neutral B. The change of internal energy as a result of the electron transfer is known as the energy defect  $\Delta E$ .

When  $\Delta E = 0$ , the process is resonant as in the case of symmetric collisions (i.e., A = B) where the cross section is well explained by semi-classical calculations over most energy ranges [12,13]. Asymmetric reactions (A  $\neq$  B) may exhibit similar behavior for reactants with small energy defects, e.g., H<sup>+</sup> + O → H + O<sup>+</sup> +  $\Delta E$  ( $\sim 0$ ) [7]. For other reactions, the energy defect is large ( $\Delta E > 0$ ) and consequently the cross section is typically smaller [14]. However, cross sections for reactions with a large  $\Delta E$  may become significant in certain high collision energy regions. When reactant B is a molecule, the number of possible reaction channels is large compared to the atomic case, and the energy dependence of the charge exchange cross section deviates from the single-peaked structure seen in asymmetric reactions such as those compiled by [15]. This is illustrated in particular by collisions between N<sub>2</sub> and atmospheric ions H<sup>+</sup> and O<sup>+</sup> in the summary of [7]. In the case of the He<sup>+</sup>-N<sub>2</sub> reaction, discrepancies still remain between a variety of experimental efforts [11,16–21], including as much as a factor of three in magnitude and qualitatively different behaviors as a function of collision energy.

Charge exchange cross sections can be measured either with a gas cell apparatus or crossed-beam apparatus. While a crossed-beam set-up more easily allows for extraction of the target products, a gas cell allows for precise measurement of the target pressure and the effective path length. For a more in-depth discussion of these two techniques, see the review by [7]. Absolute cross sections are dependent on the ability to measure the ion beam currents and neutral target pressures accurately. The experiments performed herein took place in a gas cell apparatus [22] with the goal of producing absolute cross section measurements. The gas cell was designed with a small effective path length in order to measure charge exchange cross sections with large magnitudes ( $10^{-15}$  cm<sup>2</sup>) and mitigate the problem of large angle scattering.

In Section 2, we present new measurements for the charge exchange cross sections for the near-resonant reactions between noble gas ions and N<sub>2</sub> (He<sup>+</sup>  $\Delta E = 9$  eV, Ne<sup>+</sup>  $\Delta E = 6$  eV, Ar<sup>+</sup>  $\Delta E = 0.2$  eV, Kr<sup>+</sup>  $\Delta E = -1.6$  eV) for ion energies between 0.2 and 5.0 keV. In Section 3, we present details on the updated gas cell apparatus designed to provide better absolute pressure measurements in the gas cell region and improve data taking efficiency; we also discuss future directions.

## 2. Charge Exchange with N<sub>2</sub>

### 2.1. Experimental Details

The gas cell (shown in Figure 1) is mounted on a 3D translational plus rotational ultra high vacuum (UHV) manipulator, with the intention of having the most flexibility to optimize the alignment with various ion beam sources. This so-called manipulator-mounted gas cell (MGC) includes two skimmers (1 mm and 2 mm apertures), a front end cap (3 mm aperture), a gas cell body (40 mm length), a back end cap (4 mm aperture), a retarding field analyzer (5 mm aperture), and a suppression electrode (6 mm aperture,  $-120$  V). See [22] for more details.

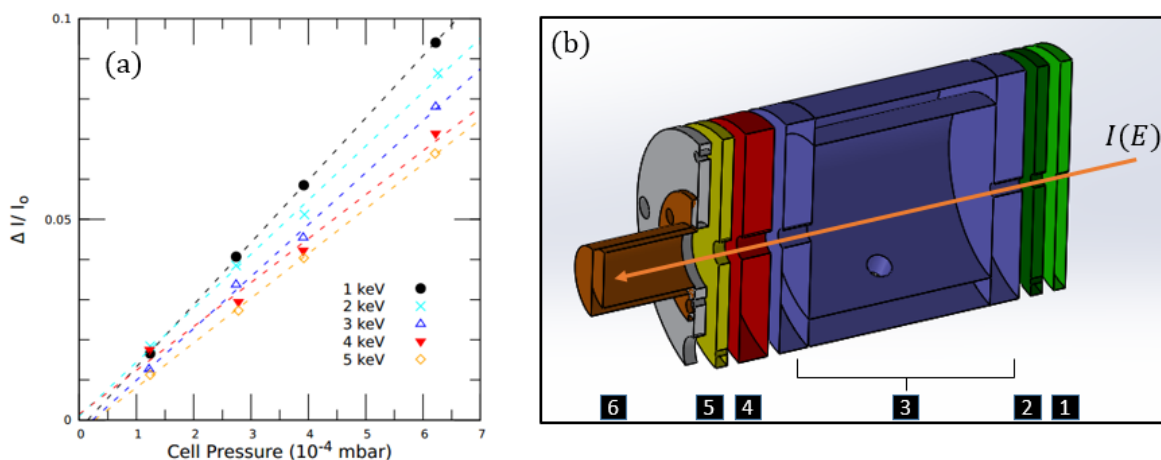


**Figure 1.** (a) Pressure-dependent current loss data obtained for the Ar<sup>+</sup> + Ar charge exchange process at incident ion energies of 1–5 keV. (b) Schematic of the gas cell used for charge exchange measurements: 1. Faceplate, 2. Skimmer, 3. Gas cell, 4. Retarding field analyzer, 5. Suppression electrode, 6. Faraday cup [22]. Reprinted from Ref. [Symmetric charge exchange for intermediate velocity noble gas projectiles. *J. Phys. B At. Mol. Opt. Phys.* **2019**, *52*, 215203], © IOP Publishing. Reproduced with permission. All rights reserved” with an appropriate reference to the other paper (<https://doi.org/10.1088/1361-6455/ab42d1>).

Beams of ions A<sup>+</sup> (A = He, Ne, Ar, Kr) are produced in an Omicron ISE 10 Sputter Ion Source. The gas cell is aligned to be colinear with the ion beam by finding the position which maximizes the current

collected in the Faraday cup. The copper Faraday cup has an aspect ratio of 0.3 to minimize errors due to secondary electrons. The acceptance angle for detection is  $2.0^\circ$  for collisions occurring near the front of the cell and  $13.0^\circ$  at the back of the cell

The measurement procedure was performed as follows: The beam current  $I_0(\epsilon)$  at each axial kinetic energy  $\epsilon$  is maximized with an empty gas cell by scanning the focal and extraction electrodes on the source for each energy studied. Then, the gas cell is filled with the target gas. The target pressure is measured with a Bayard–Alpert gauge.

After the pressure stabilizes,  $I(\epsilon)$ , the beam current with gas in the cell is measured for each of the energy values by manually adjusting the energy, focus, and extraction voltages to the values previously determined. This is repeated for four different cell pressures spaced evenly between 1 and  $8 \times 10^{-4}$  mbar. The fractional current loss,  $\frac{I_0(\epsilon) - I(\epsilon)}{I_0(\epsilon)}$ , is plotted as a function of pressure for each  $\epsilon$  and fitted to a linear function, as shown in Figure 1a. The charge exchange cross section is

$$\sigma_{cx}(\epsilon) = \frac{k_b T}{PL} \left( \frac{I_0(\epsilon) - I(\epsilon)}{I_0(\epsilon)} \right), \quad (2)$$

where  $k_b$  is the Boltzmann constant,  $T$  is the absolute temperature of the neutral gas (296 K), and  $P$  is the pressure in the gas cell.  $L$  is the effective path length of the interaction region (52.6 mm). In practice,  $\sigma_{cx}$  is calculated from the slope,  $m$ , of the fractional current loss vs. pressure graph as follows:

$$\sigma_{cx}(\epsilon) = \frac{mk_b T}{L}. \quad (3)$$

All experiments were performed in the single collision regime ( $P < 10^{-3}$  mbar) as determined by observing a strictly linear relationship between ion loss and pressure. We estimated the systematic uncertainty in the cross section at  $\pm 17\%$  and observed statistical uncertainties on the order of  $\pm 10\%$  (for more details see [22]).

## 2.2. $N_2$ Results

The charge exchange cross sections for the noble gas ions and neutral  $N_2$  are shown in Figure 2a–d. The  $He^+ + N_2$  reaction has been studied across a wide energy range [11,16–21]. All seven previous results shown in Figure 2a utilized a gas cell or similar apparatus, and all but Rudd et al. [16] and Koopman [19] were able to measure both the charged and neutral components of the ion beam post-charge exchange (CX). By looking at the slow collision products, both Koopman (1968) [19] and Stebbings [20] identified the dominant CX channel as the disassociation  $He^+ + N_2 \rightarrow He + N^+ + N$  via a two-step process.

As shown in Figure 2a, experiments at energies above 10 keV agree in trend, showing a peak at around 30 keV. For energies below 10 keV, the works of [17,19,20] show a monotonic decrease in the cross section with increasing energy. The most recent work [11] suggests a drop off toward low energies which is inconsistent with the  $He^+ - N_2$  results from [19,20]. The apparatus of Kusakabe et al. [11] is able to examine the charged and fast neutral components of their primary ion beam but are not equipped to detect the slow collision products. The measured decrease in  $\sigma_{cx}$  with decreasing energy by [11] was argued to be a consequence of the energy defect for the dissociation process,  $\Delta E \sim 0.2\text{--}0.3$  eV, which suggests a maximum in the cross section of around 0.3 keV.

Our measurements show a monotonic decrease with increasing energy; however, our cross sections are systematically higher. A voltage of  $-120$  V was applied to the suppression electrode to reflect any secondary electrons produced from the fast neutral component of the ion beam hitting the Faraday cup. Our measured cross sections include a contribution from elastic and inelastic scatter from angles above  $13^\circ$ .

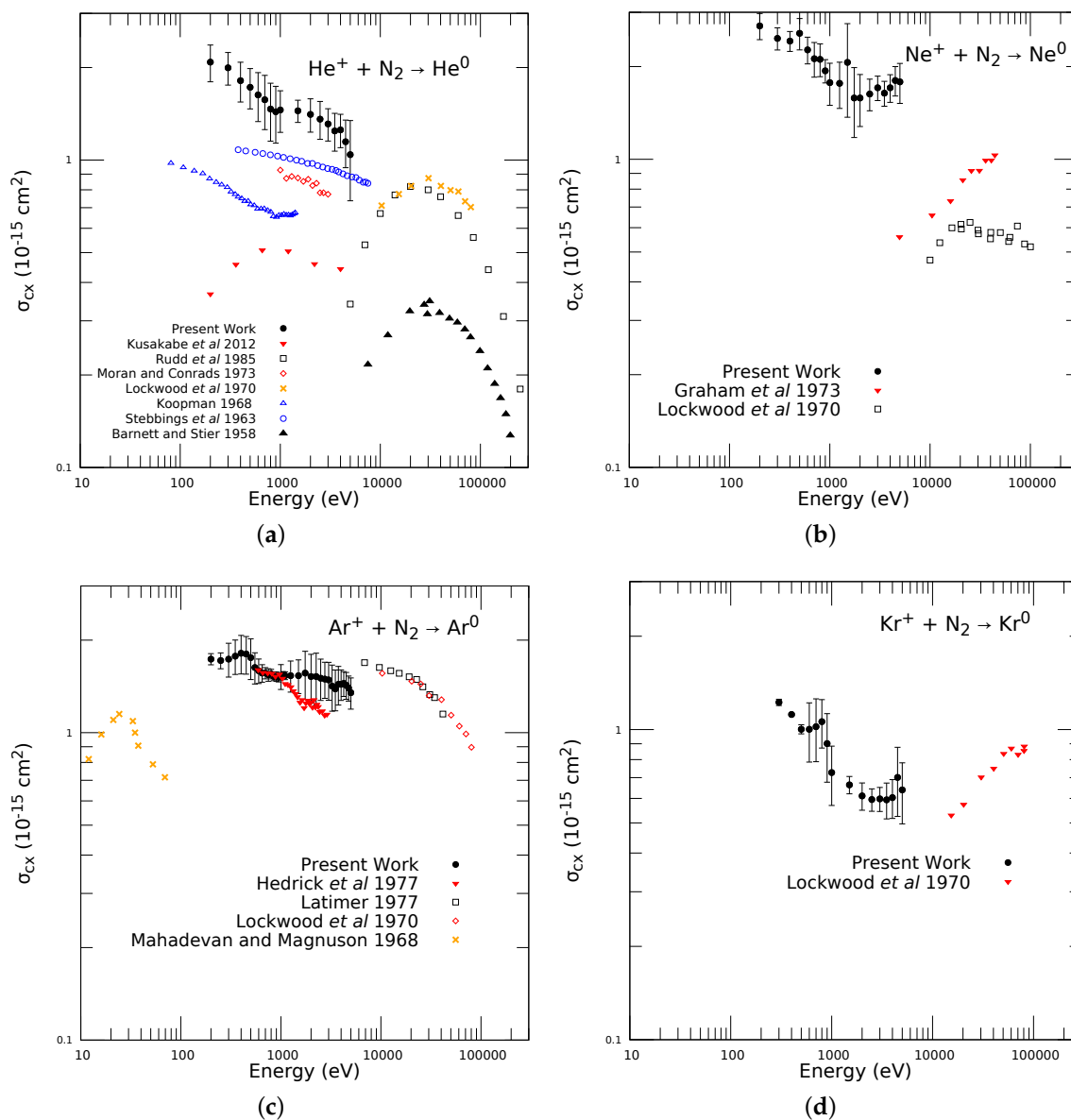


**Figure 2.** Total charge exchange cross sections for  $A^+ + \text{N}_2 \rightarrow A$  for  $A = (\text{He}, \text{Ne}, \text{Ar}, \text{Kr})$ . The error bars shown represent statistical uncertainty in the measurements. **(a)** Total charge exchange cross sections for  $\text{He}^+$  and  $\text{N}_2$ . The measurements shown: full circles (present work, manipulator-mounted gas cell (MGC)), inverted triangles [11], hollow squares [16], diamonds [17],  $\times$  [18], hollow triangles [19], open circles [20], triangles [21]. **(b)** Total charge exchange cross sections for  $\text{Ne}^+$  and  $\text{N}_2$ . The measurements shown: black circles (present work, MGC), inverted triangles [23], squares [18]. **(c)** Total charge exchange cross sections for  $\text{Ar}^+$  and  $\text{N}_2$ . The measurements shown: black circles (present work, MGC), inverted triangles [24], squares [25], diamonds [18],  $\times$  [26]. **(d)** Total charge exchange cross sections for  $\text{Kr}^+$  and  $\text{N}_2$ . The measurements shown: black circles (present work, MGC), inverted triangles [18].

For  $\text{Ne}^+ + \text{N}_2$ , only two experimental results are available [18,23]. Lockwood's cross sections [18] are nearly half an order of magnitude smaller than the present work and span an energy range outside the scope of our apparatus. The measurements by Graham et al. [23] studied the charged and neutral components of their ion beam post-CX, but their measured cross sections were placed on an absolute scale by comparison to known cross sections of protons in the respective target gases. The only point where the measurements of [23] overlap with the present work is at 5 keV where the present measurements are four times larger. As this reaction's angular dependence is unstudied, our data again include contributions from large angle elastic and/or inelastic scatter. Assuming the other works in Figure 2b isolated the charge exchange component of the total cross section, our measurements indicate that large angle non-CX scatter is comparable to CX between 0.2 and 5.0 keV.

$\text{Ar}^+ + \text{N}_2$  collisions have been studied from 0.01 to 100 keV by several groups [18,24–26]. The earliest work by [26] measured the energy distribution of both the charged and neutral component of the transmitted ion beam, and inferred the dominant reaction channel at low energy was  $\text{Ar}^+ + \text{N}_2(v = 0) \rightarrow \text{Ar} + \text{N}_2^+(v = 1) + 0.093 \text{ eV}$ . At higher energies, [24] suggests that the large number of near-resonant reaction channels leads to a relatively flat cross section as a function of energy. For measurements between 0.5 and 1 keV, we find excellent agreement between the present work and [24]. The present work and [24] have the same magnitude cross section as the higher energy results of [18,25].

For  $\text{Kr}^+ - \text{N}_2$ , only one previous work is available [18]. This paper contains measurements for all four systems studied here for energies above 10 keV. Unlike Lockwood's results in  $\text{He}^+$  and  $\text{Ar}^+$ , their data show an increase in  $\sigma_{\text{cx}}$  with increasing energy for  $\text{Kr}^+ - \text{N}_2$ . This indicates that the collision energy of the cross section maximum is higher than in the other cases. We note that of the four reactions studied here, only the  $\text{Kr}^+ - \text{N}_2$  reaction contains a negative energy defect  $\Delta E$ .

### 3. Floating Gas Cell

Having the gas cell attached to the manipulator was very useful for aligning the beam and gas cell while the apparatus was under vacuum. However, it did add some constraints to the design, specifically the pressure gauge for the gas cell being located 14 inches from the cell and connected by 1/4 inch flexible stainless steel tubing. As a result of this, it took several minutes after each pressure change for equilibration to be reached between the gas cell and the gauge. With the current ion source, each adjustment of the beam energy requires manual resetting of the three ion source voltages. The combination of manually adjusting the source and waiting for the pressure to stabilize meant that a typical measurement of 10 different energies took in the order of 1 h. As a check of the stability of the ion source, the empty-cell beam currents were again measured after the gas was pumped out of the gas cell. If significant deviations between the pre- and post-gas currents were seen, the data was discarded and retaken. Lastly, the long tubing for gas injection led to 1–2 h returns to system base pressures which were in the  $2 \times 10^{-8}$  mbar range.

A new gas cell was designed to improve the accuracy of the pressure measurements and allowed for faster data collection. A schematic of the electrically floated gas cell (FGC) is shown in Figure 3. The stainless steel gas cell body is mounted to an 8" CF flange by a hollow (1.3" internal diameter) rod. While no longer attached to the 3D manipulator for in-situ alignment, the design of the rod mount allows for the cell to be translated and rotated during installation. Alignment between the ion source exit and gas cell apertures is achieved with a HeNe laser. The hollow rod additionally provides a significantly larger conductance of the gas between the cell and the gauge. Not only is this an improvement in our ability to measure the pressure during experiments, the elimination of the narrow tubing of the MGC design results in a significant reduction in the time it takes to pump out the cell, and a reduction by a factor of four in system base pressure ( $5 \times 10^{-9}$  mbar).

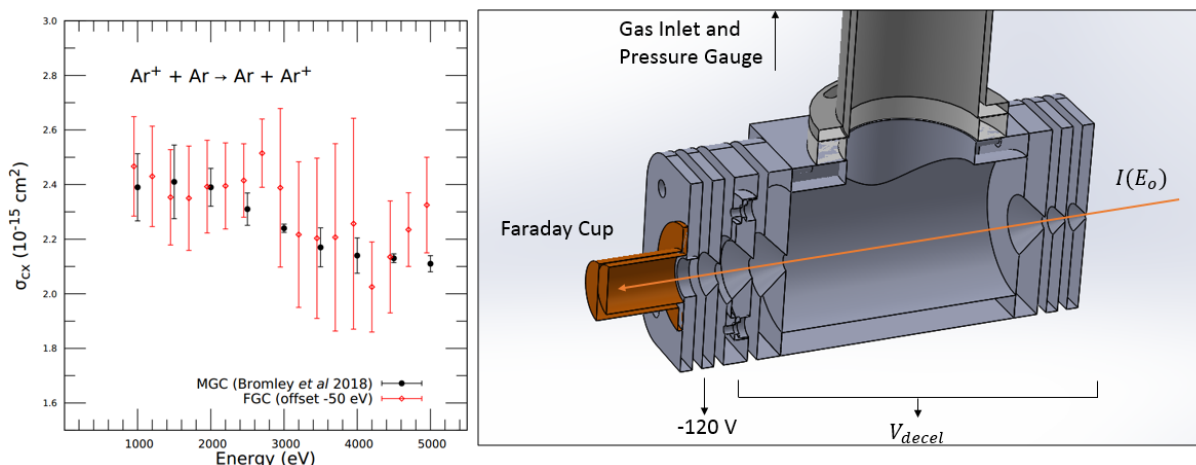


**Figure 3.** (Left) Comparison of  $\sigma_{cx}$  for  $\text{Ar}^+$  symmetric charge exchange measured with the floating gas cell (FGC) and the manipulator gas cell (MGC) from [22]. Data for the FGC is offset  $-50 \text{ eV}$  for clarity. (Right) Cut-away view of the FGC. Shown is the gas inlet, MACOR spacer (mesh not shown), and gas cell components with knife edges. The direction of the incoming beam is indicated by the orange arrow.

The dimensions and placements of the electrical components of the FGC were the same as those in the MGC except as described below. Both the faceplate and skimmer were changed from the original aperture sizes (2, 3 mm) to (1, 1 mm), respectively. The FGC electrical components, including the two skimmers, end caps, retarding field analyzer, and suppression electrode, were machined with knife edges such that scattering off of the walls of the apertures is minimized. We also modified the retarding field analyzer by adding a  $100 \times 100$  stainless steel mesh (wire thickness 0.001") in its aperture to ensure a uniform field. All components were electrically isolated with MACOR top-hat washers.

The main difference, however, is that the gas cell is electrically isolated from the gas inlet (and therefore the rest of the vacuum chamber) by a 1/4" thick MACOR ring. On the underside of the MACOR ring, a thin annular holder braces a titanium mesh ( $20 \times 20$ , wire diameter 0.016") between the MACOR ring and cell body. Teflon sleeves insulate the screw heads between the cell body and metal gas inlet. With the FGC, rather than adjusting the beam energy  $\epsilon$  at the ion source as in the MGC design, the FGC beam energy is adjusted by applying an electric potential  $V_{FGC}$  to all of the gas cell components (i.e., skimmers, end caps, cell body, and retarding field analyzer). This was done using a digitally controlled high voltage supply integrated into our system's LabVIEW control software. The beam energy in the cell is then given by  $\epsilon = |e|(V_{source} - V_{FGC})$ .

The experimental procedure was the same as previously described except that the parameters of the ion beam source were fixed providing a single source energy throughout an experiment. After recording data for a series of beam energies and cell pressures, the analysis was done using Equation (3), the same as with the MGC data. In Figure 3, we can see a comparison of the measurements of the  $\text{Ar}^+$ -Ar cross section in the MGC [22] and preliminary tests using the FGC. For the  $\text{Ar}^+$ -Ar measurements from the MGC [22] in Figure 3, the statistical uncertainties are in the order of  $\pm 5\%$ . In the FGC data, the statistical uncertainties in the cross sections are in the order of  $\pm 9\%$ . The use of 1 mm apertures in both the faceplate and skimmer decrease the beam current significantly compared to the MGC design ( $I_0^{MGC} \sim 10\text{--}60 \text{ nA}$ ,  $I_0^{FGC} \sim 2\text{--}10 \text{ nA}$ , depending on ion source pressure and beam energy), and the smaller beam currents lead to larger noise in the Faraday cup current measurements.

It is important to note that with the MGC design, one experimental set (consisting of 10 energies each) either spanning 0.2–1.0 keV or 1.0–5.0 keV, took 3 h due to the long pumping times (up to 2 h) and the measurement duration (1 h). With the FGC design, one experimental set, spanning 2 keV in  $E$ , may be

accomplished in 0.5 h, and thus a single reaction in Figure 2 may be accomplished in 8 h (breaking the energy range in two sections and performing each four times). Increasing the ion source operating pressure and/or reverting the faceplate and skimmer apertures to their original sizes (2, 3 mm) would increase the measured beam currents and reduce the statistical uncertainties in the measured cross sections.

#### 4. Conclusions

We measured total charge exchange cross sections for the reactions  $A^+ + N_2 \rightarrow A$  for ions  $A = (\text{He}, \text{Ne}, \text{Ar}, \text{Kr})$  between 0.2 and 5.0 keV. From comparisons with other measurements in  $N_2$ , our results suggest large-angle scattering may be important in ion-molecule scattering in the keV energy range. Presently, the MGC design cannot distinguish between current loss due to scatter beyond  $13^\circ$  and neutralization of ions from CX. Future experiments will investigate the effect of larger aperture sizes on the measured cross sections. Increasing the aperture sizes of the back end cap from 4 to 6 mm and the Faraday cup, suppression electrode, and retarding field analyzer to 9 mm will yield an increase in the collection angle from  $2^\circ$  (present) to  $4^\circ$  at the front of the cell and from  $13^\circ$  (present) to  $18^\circ$  at the rear of the cell. In total, this change will increase the effective collection area of our primary ion beam and help constrain the effect of scattering to large angles in these noble gas ion-molecule collisions.

The design and first measurements with an electrically floating gas cell were also presented. Preliminary results with this new design are in excellent agreement with previous measurements from our group, but also show larger statistical uncertainties. However, the faster measurement protocol means that we can compensate by taking more measurements. Other methods for increasing the signal to noise will include increasing the ion beam current density and/or working with larger aperture radii.

**Author Contributions:** C.S. and J.M. contributed to the design of the apparatus and oversaw the experimental program. C.A. designed the Floating Gas Cell. S.B. carried out construction and testing of the Floating Gas Cell. All experimental measurements and data analysis were carried out by S.B. All authors contributed to preparing this manuscript.

**Acknowledgments:** The authors gratefully acknowledge the work of the Physics and Astronomy Instrumentation Shop and financial support from the Clemson University College of Science.

**Conflicts of Interest:** The authors declare no conflict of interest.

#### Abbreviations

The following abbreviations are used in this manuscript:

CX	charge exchange
FGC	Floated Gas Cell
MGC	Manipulator Gas Cell

#### References

1. Janev, R.; Harrison, M.; Drawin, H. Atomic and molecular database for fusion plasma edge studies. *Nucl. Fusion* **1989**, *29*, 109. [[CrossRef](#)]
2. Schwadron, N.A.; Cravens, T.E. Implications of Solar Wind Composition for Cometary X-rays. *Astrophys. J.* **2000**, *544*, 558. [[CrossRef](#)]
3. Fabian, A.C.; Sanders, J.S.; Williams, R.J.R.; Lazarian, A.; Ferland, G.J.; Johnstone, R.M. The energy source of the filaments around the giant galaxy NGC 1275. *Mon. Not. R. Astron. Soc.* **2011**, *417*, 172–177. [[CrossRef](#)]
4. Bhardwaj, A.; Dhanya, M.B.; Alok, A.; Barabash, S.; Wieser, M.; Futaana, Y.; Wurz, P.; Vorburgen, A.; Holmström, M.; Lue, C.; et al. A new view on the solar wind interaction with the Moon. *Geosci. Lett.* **2015**, *2*, 10. [[CrossRef](#)]

5. Mullen, P.D.; Cumbee, R.S.; Lyons, D.; Gu, L.; Kaastra, J.; Shelton, R.L.; Stancil, P.C. Line Ratios for Solar Wind Charge Exchange with Comets. *Astrophys. J.* **2017**, *844*, 7. [[CrossRef](#)]
6. Roble, R.G.; Ridley, C.C. An auroral model for the NCAR thermospheric general circulation model (TGCM). *Ann. Geophys. A* **1987**, *5*, 369–382.
7. Lindsay, B.G.; Stebbings, R.F. Charge transfer cross sections for energetic neutral atom data analysis. *J. Geophys. Res.* **2005**, *110*, A12213. [[CrossRef](#)]
8. Larsson, M.; Geppert, W.D.; Nyman, G. Ion chemistry in space. *Rep. Prog. Phys.* **2012**, *75*, 066901. [[CrossRef](#)]
9. Bodewits, D.; Hoekstra, R.; Seredyuk, B.; McCullough, R.W.; Jones, G.H.; Tielens, A.G.G.M. Charge Exchange Emission from Solar Wind Helium Ions. *Astrophys. J.* **2006**, *642*, 593. [[CrossRef](#)]
10. Werbowy, S.; Pranszke, B. Charge-exchange processes in collisions of  $H^+$ ,  $H_2^+$ ,  $H_3^+$ ,  $He^+$ , and  $He_2^+$  ions with CO and  $CO_2$  molecules at energies below 1000 eV. *Phys. Rev. A* **2016**, *93*, 022713. [[CrossRef](#)]
11. Kusakabe, T.; Kitamuro, S.; Nakai, Y.; Tawara, H.; Sasao, M. Charge-Transfer Cross Sections of Ground State  $He^+$  Ions in Collisions with He Atoms and Simple Molecules in the Energy Range below 4.0 keV. *Plasma Fusion Res.* **2012**, *7*, 2401062. [[CrossRef](#)]
12. Rapp, D.; Francis, D.E. Charge Exchange between Gaseous Ions and Atoms. *J. Chem. Phys.* **1962**, *37*, 2631–2645. [[CrossRef](#)]
13. Hodgkinson, D.P.; Briggs, J.S. Resonant charge exchange at low velocities. *J. Phys. B At. Mol. Phys.* **1976**, *9*, 255. [[CrossRef](#)]
14. Massey, H.S.W. Collisions between atoms and molecules at ordinary temperatures. *Rep. Prog. Phys.* **1949**, *12*, 248. [[CrossRef](#)]
15. Friedman, B.; DuCharme, G. Semi-empirical scaling for ion-atom single charge exchange cross sections in the intermediate velocity regime. *J. Phys. B At. Mol. Opt. Phys.* **2017**, *50*, 115202. [[CrossRef](#)]
16. Rudd, M.E.; Goffe, T.V.; Itoh, A. Cross sections for ionization of gases by 10–2000 keV  $He^+$  ions and for electron capture and loss by 5–350 keV  $He^+$  ions. *Phys. Rev. A* **1985**, *32*, 829–835. [[CrossRef](#)]
17. Moran, T.F.; Conrads, R.J. Charge neutralization of  $He^+$  ion beams. *J. Chem. Phys.* **1973**, *58*, 3793–3799. [[CrossRef](#)]
18. Lockwood, G.J. Total Cross Section for Charge Transfer of Noble-Gas Ions  $N_2$ . *Phys. Rev. A* **1970**, *2*, 1406–1410. [[CrossRef](#)]
19. Koopman, D.W. Light-Ion Charge Exchange in Atmospheric Gases. *Phys. Rev.* **1968**, *166*, 57–62. [[CrossRef](#)]
20. Stebbings, R.F.; Smith, A.C.H.; Ehrhardt, H. Dissociative Charge Transfer in  $He^+O_2$  and  $He^+N_2$  Collisions. *J. Chem. Phys.* **1963**, *39*, 968–971. [[CrossRef](#)]
21. Barnett, C.F.; Stier, P.M. Charge Exchange Cross Sections for Helium Ions in Gases. *Phys. Rev.* **1958**, *109*, 385–390. [[CrossRef](#)]
22. Bromley, S.J.; Fox, D.C.; Sosolik, C.E.; Harriss, J.E.; Marler, J.P. A gas cell apparatus for measuring charge exchange cross sections with multicharged ions. *Rev. Sci. Instrum.* **2018**, *89*, 073107. [[CrossRef](#)] [[PubMed](#)]
23. Graham, W.G.; Latimer, C.J.; Browning, R.; Gilbody, H.B. Ionization of fragmentation of diatomic molecular gases by 5–45 keV  $Ne^+$  and  $Na^+$  ions and Ne atoms. *J. Phys. B At. Mol. Phys.* **1973**, *6*, 2641–2652. [[CrossRef](#)]
24. Hedrick, A.F.; Moran, T.F.; McCann, K.J.; Flannery, M.R. Charge transfer cross sections in argon ion–diatomic molecule collisions. *J. Chem. Phys.* **1977**, *66*, 24–31. [[CrossRef](#)]
25. Latimer, C.J. Near-resonant charge transfer in collisions of rare-gas ions with simple molecules within the energy range 4–45 keV. *J. Phys. B At. Mol. Phys.* **1977**, *10*, 515–522. [[CrossRef](#)]
26. Mahadevan, P.; Magnuson, G.D. Low-Energy (1- to 100-eV) Charge-Transfer Cross-Section Measurements for Noble-Gas-Ion Collisions with Gases. *Phys. Rev.* **1968**, *171*, 103–109. [[CrossRef](#)]

